J. Fluid Mech. (2012), *vol.* 712, *pp.* 451–470.
doi:10.1017/jfm.2012.432

Exact Floquet theory for waves over arbitrary periodic topographies

Jie Yu[1]† **and Louis N. Howard**[2]

[1] Department of Civil, Construction and Environmental Engineering, North Carolina State University, Raleigh, NC 27695-7908, USA

[2] Department of Mathematics, Massachusetts Institute of Technology, Cambridge, MA 02139, USA

(Received 18 February 2012; revised 3 July 2012; accepted 28 August 2012;
first published online 28 September 2012)

We consider linear waves propagating over periodic topographies of arbitrary amplitude and wave form, generalizing the method in Howard & Yu (*J. Fluid Mech.*, vol. 593, 2007, pp. 209–234). By a judicious construction of a conformal map from the flow domain to a uniform strip, exact solutions of Floquet type can be developed in the mapped plane. These Floquet solutions, in an essentially analytical form, are analogous to the complete set of flat-bottom propagating and evanescent waves. Therefore they can be used as a basis for the solutions of boundary value problems involving a wavy topography with a constant mean water depth. Various concrete examples are given and quantitative results are discussed. Comparisons with experimental data are made, and qualitative agreement is achieved.

Key words: coastal engineering, surface gravity waves, wave scattering

1. Introduction

In 2007 we published a paper (Howard & Yu 2007, hereafter referred to as HY07), showing how exact solutions can be constructed for linear waves over large periodic bottom corrugations, capable of describing both the slowly and fast varying aspects of the flow. This was to some degree extended in Yu & Howard (2010, hereafter referred to as YH10). In both of these papers, we made use of a particular family of bottom profiles because of the existence of simple familiar formulas for a conformal map of the flow domain to a uniform strip. The question has been raised since then of whether these exact solutions are restricted to the special choice of the bed form. The purpose of this paper is to generalize the exact theory, considering periodic topographies of arbitrary amplitude and wave form.

Wave propagation over variable topographies has long been of interest to scientists and engineers, due to its importance in coastal and oceanographic applications. The mathematical difficulty for problems of this kind is evident: even for linear waves over a simple regular periodic topography, there are few exact analytical solutions. Consequently, a wide range of approximate theories has been developed, using various techniques and making various hypotheses, such as small bottom amplitude (or other geometry constraints), slowly varying waves, etc.; for large bottom amplitude, numerical, or semi-numerical, methods have generally been sought (see the discussion

† Email address for correspondence: jie_yu@ncsu.edu

in Athanassoulis & Belibassakis 1999, and references therein). Problems involving periodic topographies have been extensively studied, in particular since the work of Davies (1982) and Heathershaw (1982), due to the interest in Bragg resonance (when the water wavelength is twice the bottom wavelength). For rapidly varying topographies, one approach is to discretize the bottom into small pieces of horizontal steps, on each of which the solution is represented as a linear combination of the flat-bottom waves and evanescent modes appropriate to the local depth. The proportion coefficients are solved numerically by matching the flow conditions at the boundaries between the sections, together with suitable conditions at the ends of the variable bed region: see Devillard, Dunlop & Souillard (1988), O'Hare & Davies (1992) and Rey (1992), among many others. The computational cost can be high depending on the discretization and the number of modes needed. A similar approach is to superpose the flat-bottom modes with spatially varying proportion coefficients, which are coupled and described by a system of ordinary differential equations (upon applying a variational principle or Galerkin method, for example). A significant improvement to this method has been provided by Athanassoulis & Belibassakis (1999), who included a sloping-bottom mode to amend the shortcoming in satisfying the bottom boundary condition by the flat-bottom modes.

In an approach superficially similar to the piecewise bed approach in its use of transfer matrices to combine individual sections, Porter & Porter (2003) formulated a series of problems for scattering by a single bed period. The extended scattering matrix for linking N periods of the bed involves the solution to a system of integral equations, which arises from the use of flat-bottom propagating and evanescent waves to construct the Green's function for a bed period. The computation of particular solutions is done by numerically solving the integral equations using the Galerkin approximation. Results are given for particular cases of (i) scattering by a finite length of periodic bed, (ii) waves analogous to Bloch waves in a crystal (which exist on an infinite domain), and (iii) a low normal mode of a rectangular tank with periodic bottom. (HY07 also treats normal modes of such a tank, but emphasizes relatively high modes where effects of Bragg resonance are significant.)

In this paper, we extend the idea of HY07 to develop an exact theory for linear time periodic motions over a general periodic topography without any constraint on the undulation amplitude and shape, seeking the Floquet type of solutions in a conformally mapped plane. Making use of the periodicity of the problem, we represent the required conformal map as a Fourier series. The coefficients of the series are computed iteratively, given a bed profile. The algorithm used in the present paper is very effective for smooth functions, but becomes less so for non-smooth functions with large bottom amplitude, for instance the square-wave bottom profile (with rounded corners: see § 3). More efficient algorithms for extreme cases can certainly be found, but we do not pursue them here.

The Floquet solutions, of Laplace's equation and vertical boundary conditions, consist of a family of two wave modes and two infinite families of evanescent modes. These are completely analogous – but not identical – to the propagating and evanescent waves on a flat bottom. They can be used to construct solutions to various boundary value problems involving a wavy seabed (with a constant mean water depth), in a way similar to the use of the flat-bottom solutions. Applications of the solutions in HY07 and YH10 have been made there to the normal mode problem of a tank with a corrugated bottom, and more recently to wave propagation over a patch of bottom corrugations in an otherwise flat seabed (Yu & Zheng 2012; see also Zheng 2011).

It should be mentioned that Nachbin (1995) used a numerical conformal transformation of Schwarz–Christoffel type to consider randomly rapidly varying topographies, extending the earlier work on linear waves in shallow water (Nachbin & Papanicolaou 1992). Evans & Linton (1994) considered conformal transformation to a uniform strip prior to applying a discretization technique essentially similar to Devillard *et al.* (1988).

This paper is organized as follows. In § 2 the formulation of the problem is presented, including the construction of the conformal transformation functions and the Floquet solutions for time periodic motions in the mapped plane. The analogy and connection of the Floquet solutions to the flat-bottom propagating and evanescent modes are discussed in § 3, where quantitative results are also shown and discussed using examples of bottom profiles, such as the doubly sinusoidal and square wave (with rounded corners) bottoms. Remarks on water wave Bragg reflections are made in § 4, clarifying the interpretation of higher-order ($m > 1$) reflections (occurring when the water wavelength is close to $2/m$ times the bottom wavelength, $m = 2, 3, \ldots$) and the so-called first-order ($m = 1$) reflection of the mth Fourier components of a bed profile. Comparisons with experimental data are also attempted. Summarizing remarks follow in § 5.

2. Linear irrotational motions on a periodic seabed

Consider ideal fluids in the vertical plane (x, z). Let the seabed be at $z = -h_0 + h_b(x)$, where h_0 is a constant, and let the undisturbed free surface be $z = 0$. For linear inviscid irrotational motions, the velocity potential ϕ is described by the following equations:

$$\nabla^2\phi = 0 \quad \text{for } -h_0 + h_b(x) \leqslant z \leqslant 0, \ -\infty < x < \infty, \tag{2.1}$$

$$\phi_z = \phi_x h_{b,x} \quad \text{at } z = -h_0 + h_b(x), \tag{2.2}$$

$$\phi_{tt} + g\phi_z = 0 \quad \text{at } z = 0. \tag{2.3}$$

We consider $h_b(x)$ to be a periodic function of arbitrary shape and amplitude. The only constraint is that $h_b(x)$ has zero average in x, so that the mean water depth is given by h_0. Let λ_{bar} be a period such that $h_b(x + \lambda_{bar}) = h_b(x)$, hence the bottom wavenumber $k_{bar} = 2\pi/\lambda_{bar}$. (Although λ_{bar} may often be chosen to be the fundamental period, i.e. the shortest distance that the bed form repeats, it is not required.) We define a water wavenumber

$$k_B = \pi/\lambda_{bar}, \tag{2.4}$$

i.e. $k_B = k_{bar}/2$. We shall use k_B for normalization to make the bottom undulations π-periodic, following the general practice in Mathieu's equation. Even though it does not appear explicitly, the solution to linear motions over bottom corrugations has features similar to those of solutions of Mathieu's equation (YH10). Specifically, the general idea of Floquet solutions applies here as well, as will be seen in § 2.2.

2.1. *The conformal map*

As in HY07, we wish to find a conformal transformation which maps the undisturbed flow domain $-h_0 + h_b(x) \leqslant z \leqslant 0$, $-\infty < x < \infty$ onto a uniform strip $-k_B h \leqslant \eta \leqslant 0$, $-\infty < \xi < \infty$, where $\eta = -k_B h$ is the flat bottom in the mapped plane. Since the velocity potential is still given by a Laplace equation, exact solutions become attainable in the mapped plane due to the simple geometry of the boundaries (straight lines).

Suppose we write the mapping functions $x(\xi, \eta)$ and $z(\xi, \eta)$ in Fourier series,

$$k_B x = \xi - \epsilon k_B h \sum_{j=1}^{\infty} \left(b_j \sin 2j\xi - c_j \cos 2j\xi\right) \cosh(2j\eta) / \sinh(2jk_B h), \tag{2.5}$$

$$k_B z = \eta - \epsilon k_B h \sum_{j=1}^{\infty} \left(b_j \cos 2j\xi + c_j \sin 2j\xi\right) \sinh(2j\eta) / \sinh(2jk_B h), \tag{2.6}$$

where b_j and c_j are both real, yet to be determined. The dimensionless parameter ϵ is a measure of the bottom amplitude relative to the mean water depth h_0, and is not necessarily small. The Cauchy–Riemann conditions, $\partial x/\partial\xi = \partial z/\partial\eta$, $\partial x/\partial\eta = -\partial z/\partial\xi$, can be verified by inspection; so this is indeed a conformal transformation. It is clear that $z = 0$ is mapped onto $\eta = 0$. By requiring the seabed $z = -h_0 + h_b(x)$ to be mapped onto $\eta = -k_B h$, we obtain from (2.5) and (2.6)

$$h_b(x) = (h_0 - h) + \epsilon h \sum_{j=1}^{\infty} \left(b_j \cos 2j\xi + c_j \sin 2j\xi\right), \tag{2.7}$$

$$k_B x = \xi - \epsilon k_B h \sum_{j=1}^{\infty} \left(b_j \sin 2j\xi - c_j \cos 2j\xi\right) \coth 2jk_B h, \tag{2.8}$$

which is a parametric representation of the bottom profile $h_b(x)$. This enables us to determine the Fourier coefficients b_j and c_j, given a function $h_b(x)$, hence finding the conformal transformation (2.5) and (2.6) with the designated purpose. For a periodic function of arbitrary shape and amplitude, such a parametric representation in (2.7) and (2.8) can always be found, as long as $h_b(x)$ can be represented by a Fourier series. It is clear that $h_b(x)$ is π-periodic both in ξ and in $k_B x$. The water depth h in the mapped plane is determined by requiring the right-hand side of (2.7) to have a zero mean in $k_B x$, i.e.

$$h + \epsilon^2 k_B h^2 \sum_{j=1}^{\infty} j \left(b_j^2 + c_j^2\right) \coth(2jk_B h) = h_0. \tag{2.9}$$

Clearly, $h < h_0$. Figure 1 shows the geometry of an undisturbed flow domain in the physical plane (x, z), and the corresponding uniform strip in the mapped plane (ξ, η), indicating the water depths h_0 and h. It is also seen from (2.7) and (2.8) that when $c_j = 0$, the bottom profile is symmetric in ξ, as well as in $k_B x$. An example of a symmetric profile can be seen in the cusp-like bottom corrugations in HY07 and YH10.

It follows from the Riemann mapping theorem that any strip-like region, such as the flow domain under consideration here (with a flat top and undulating bottom), can be conformally mapped onto the strip of uniform depth and with a suitable normalization in a unique way (Ahlfors 1953). When the bottom is periodic, so that it can be (with very mild restrictions) represented by a Fourier series, this representation can always be used to construct the conformal map, as described above. Given a profile $h_b(x)$, we can solve for b_j and c_j from (2.7) and (2.8), using an iterative method which involves applying the discrete Fourier transform in ξ repeatedly. Details of the numerical scheme are given in appendix B.

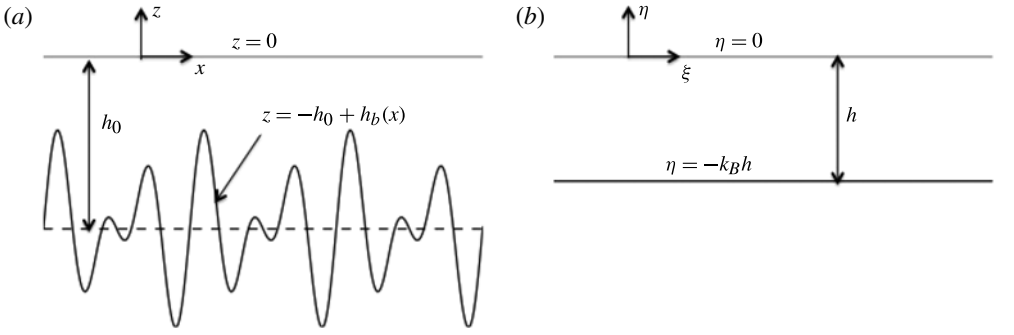

FIGURE 1. A sketch of the undisturbed flow domain, showing relevant parameters in (*a*) the physical plane (x, z) and (*b*) the mapped plane (ξ, η).

2.2. *The Floquet solutions*

For a time periodic solution, $\phi = \varphi e^{-i\omega t} + \text{c.c.}$, where ω is the angular frequency of the simple harmonic waves. In the mapped plane (ξ, η), we write from (2.1)–(2.3)

$$\varphi_{\xi\xi} + \varphi_{\eta\eta} = 0 \quad \text{for} \quad -k_B h \leqslant \eta \leqslant 0, \quad -\infty < \xi < \infty, \tag{2.10}$$

$$\varphi_\eta = 0 \quad \text{at} \quad \eta = -k_B h, \tag{2.11}$$

$$\varphi_\eta = \sigma^2 \left(1 - 2\epsilon k_B h \sum_{j=1}^{\infty} \frac{\left(b_j \cos 2j\xi + c_j \sin 2j\xi\right) j}{\sinh(2jk_B h)}\right) \varphi \quad \text{at} \quad \eta = 0, \tag{2.12}$$

where

$$\sigma = \omega/\sqrt{gk_B} \tag{2.13}$$

is the dimensionless frequency. The solutions to (2.10)–(2.12) are of Floquet type (HY07), i.e.

$$\varphi(\xi, \eta; \mu) = e^{\mu\xi} P(\xi, \eta; \mu), \tag{2.14}$$

and

$$P(\xi, \eta; \mu) = \sum_{n=-\infty}^{\infty} D_n e^{in\xi} \frac{\cosh\left[(n - i\mu)(\eta + k_B h)\right]}{\cosh\left[(n - i\mu) k_B h\right]} \tag{2.15}$$

is the periodic factor with period of π or 2π in ξ. The Floquet exponent μ and Fourier coefficients $D_n(\mu)$ satisfy

$$L_n D_n = \sum_{j=1}^{\infty} D_{n-2j}\Theta_j^- + D_{n+2j}\Theta_j^+, \tag{2.16}$$

$$\Theta_j^{\pm} = j\left(b_j \pm ic_j\right) \sinh(2k_B h)/\sinh(2jk_B h), \tag{2.17}$$

$$L_n := (\epsilon k_B h)^{-1} \sinh(2k_B h) \left\{1 - \sigma^{-2}(n - i\mu) \tanh\left[(n - i\mu) k_B h\right]\right\}. \tag{2.18}$$

The recurrence relation (2.16) comes from the free surface condition (2.12), where the effects of the bottom on the wave are seen upon the transformation to (ξ, η). It is of course also the periodic coefficients in (2.12) that make the Floquet theory relevant here.

The individual terms of the sum (2.15) are obviously solutions of the Laplace equation (2.10) and the bottom boundary condition (2.11). They are not individually solutions of the top boundary condition (2.12), but the sum is (together with the factor $e^{\mu\xi}$), provided the Fourier coefficients $D_n(\mu)$ and the Floquet exponent μ satisfy (2.16) with the definitions (2.17) and (2.18). Although it is superficially similar to the elementary separation of variables techniques, which can be used for the flat-bottom case ($\epsilon = 0$), we cannot obtain here the ordinary type of Sturm–Liouville eigenvalue problem in the vertical direction. This is because the top boundary condition (2.12) contains the horizontal variable ξ when $\epsilon \neq 0$. Instead, we get the problem of finding μ so that the homogeneous system (2.16) has non-trivial solutions. This leads to Hill's determinant and associated ideas discussed in § 2.3. A few points are worth making.

First, we note that Θ_j^+ and Θ_j^- are complex conjugates and completely determined by the properties of the map, being independent of the frequency σ and Floquet exponent μ. The definition of L_n is the same as in HY07, and $L_n(-\mu) = L_{-n}(\mu)$ for any μ.

Second, from (2.16) it is seen that D_n for even and odd n do not couple. This is due to the fact that the coefficients in (2.12) are π-periodic, a common feature in Mathieu's equation. One can choose to use either an even or odd representation in (2.14). An even representation can be made into an odd representation by replacing μ with $\mu - \mathrm{i}$ or $\mu + \mathrm{i}$, and vice versa. Without any loss of generality, and to suppress this apparent non-uniqueness in representing the solution, we shall require $-1 < \mathrm{Im}(\mu) \leqslant 1$ (HY07).

Third, there are some symmetry properties which can be used to advantage in computation. For real μ, $L_{-n}(\mu) = L_n^*(\mu)$ and $D_n(\mu) = D_{-n}^*(\mu)$, where $*$ stands for complex conjugate; hence $\varphi(\mu)$ is real. For pure imaginary μ, $L_n(\mu)$ are real and $D_n^*(-\mu) = D_{-n}(\mu)$; thus $\varphi(-\mu) = \varphi^*(\mu)$. For symmetric bottom profiles, $c_j = 0$ and $\Theta_j^+ = \Theta_j^-$, and are real. In this case, $D_n(-\mu) = D_{-n}(\mu)$ for real μ and the periodic factor for $-\mu$ is the complex conjugate of that for μ; for pure imaginary μ, D_n are real (or can be scaled to be so) and $D_n(-\mu) = D_{-n}(\mu)$, so the periodic factor is the same for μ and $-\mu$.

2.3. *The 'dispersion relationship' $\mu(\sigma)$*

The crux of the problem is to determine the Floquet exponents μ. Let $\boldsymbol{X}$ be the vector whose elements are D_n. The homogeneous system (2.16) is written as $\boldsymbol{AX} = 0$, where $\boldsymbol{A}$ is a square matrix. For example, for $n =$ odd and

$$\boldsymbol{X} = [\cdots \; D_{-3} \;\; D_{-1} \;\; D_1 \;\; D_3 \;\; \cdots]^{\mathrm{T}}, \tag{2.19}$$

where T stands for transpose,

$$\boldsymbol{A} = \begin{pmatrix} \cdots & \cdots & \cdots & \cdots & \cdots & \cdots \\ \cdots & L_{-3} & -\Theta_1^+ & -\Theta_2^+ & -\Theta_3^+ & \cdots \\ \cdots & -\Theta_1^- & L_{-1} & -\Theta_1^+ & -\Theta_2^+ & \cdots \\ \cdots & -\Theta_2^- & -\Theta_1^- & L_1 & -\Theta_1^+ & \cdots \\ \cdots & -\Theta_3^- & -\Theta_2^- & -\Theta_1^- & L_3 & \cdots \\ \cdots & \cdots & \cdots & \cdots & \cdots & \cdots \end{pmatrix}. \tag{2.20}$$

The infinite determinant of $\boldsymbol{A}$ is a function of σ and μ, given the properties of the map. Denoting $\Delta(\mu, \sigma) \equiv \det(\boldsymbol{A})$, the determinantal equation

$$\Delta(\mu, \sigma) = 0 \tag{2.21}$$

determines the possible Floquet exponents μ given a frequency σ. This relationship is similar to that for Hill's equation, from which Hill's infinite determinants are named. (In Mathieu's equation, $\boldsymbol{A}$ is tri-diagonal.) For a typical Hill's determinant, the issues of convergence and the solutions are well studied (Whittaker & Watson 1927). Convergence of such an infinite determinant is not particularly relevant here, because the determinant can be made to converge by multiplying rows and columns by suitable non-zero factors, which will affect neither the roots of (2.21) nor the method of the solutions (Jeffreys & Jeffreys 1950). In the present problem, $\sum \Theta_j^{\pm}$ is absolutely convergent, as b_j and c_j are the Fourier coefficients of the bottom profile. In fact, the behaviour of $\Theta_j^{\pm}$ at large j is dominated by $1/\sinh(2jk_Bh)$: see (2.17). Even if the bed profile has a jump discontinuity, b_j and c_j converge as $1/j$. It is then seen from (2.17) that an overall bound of at worst $\Theta_j^{\pm} \sim \mathrm{e}^{-2jk_Bh}$ can be expected. The diagonal elements L_n behave as $(n - \mathrm{i}\mu)$ for large n. To solve (2.21), we can normalize the diagonal elements to be 1 for the convergence. For pure imaginary μ and $\mu = 0$, $\Delta(\mu, \sigma)$ is real since $\boldsymbol{A}$ is Hermitian. For real μ, $\Delta(\mu, \sigma)$ is also real due to the symmetry in $\boldsymbol{A}$: see appendix A. Once μ is determined, the D_n are given by the vector in the null space of $\boldsymbol{A}$.

We shall refer to (2.21) as the 'dispersion relation' for linear modes over a wavy bottom. In both the elementary water wave theory and for Floquet solutions over a periodical bed, we are dealing with temporally sinusoidal motions of a definite frequency ω. But the Floquet solutions cannot really be said to have a 'wavenumber', unless $\mu = 0$. They are not spatially sinusoidal, nor are they usually even spatially periodic. The Floquet form of the solutions is, however, analogous to the ordinary planar wave theory, and it seems appropriate to call the relation between temporal frequency and the exponent μ by the same name.

3. Discussion

The Floquet solution, given in (2.14) and (2.15), is not a particular solution. It represents a set of solutions, individually identified by the Floquet exponents μ. The behaviour of these Floquet solutions as $\epsilon \to 0$ can be followed either numerically or by treating (2.12) as a perturbation in ϵ, taking either a flat-bottom propagating or evanescent mode as the zero state. Alternatively, one can carry out the perturbation in ϵ of the matrix $\boldsymbol{A}$ and (2.21). This is the approach adapted in YH10, in which $\boldsymbol{A}$ is tri-diagonal and $\det(\boldsymbol{A})$ can be written as a continued fraction due to the simple conformal transformation associated with the bottom profile used.

For a given temporal frequency ω there is a Floquet exponent μ (and its negative), which tends to zero as $\epsilon \to 0$ while the associated solution approaches a flat-bottom propagating wave (or standing wave if ω is a flat-bottom Bragg resonance frequency). It thus seems appropriate to refer to these motions as wave modes. For these modes, μ is found to be either real or pure imaginary, depending on whether ω is inside or outside a resonance wedge (HY07, YH10). In addition to these, for the given ω we also find an infinite family of μ (and their negatives) which are real and approach the eigenvalues (non-zero) of evanescent waves of a flat bottom as $\epsilon \to 0$. These are referred to as Floquet evanescent modes. It should be noticed that for wave modes with real μ, the wave amplitude modulates exponentially in space due to the factor $\mathrm{e}^{\mu\xi}$, but much more slowly. This is quite different from the evanescent modes, which are characterized by rapid exponential variation in ξ due to the large values of μ.

It is well known that the complete set of flat-bottom eigenfunctions consists of two wave modes (left- and right-propagation) and two families of evanescent modes, each

of which has infinite numbers. These modes form the basis for constructing solutions to various boundary value problems. Using the Floquet solutions in (2.14)–(2.18), a complete set of analogues can be found: that is, as $\epsilon \to 0$, the set of Floquet solutions approaches the complete set of the flat-bottom linear modes for the given frequency ω. It is therefore clear that the Floquet solutions in (2.14)–(2.18) can be used as the basis for solutions to boundary value problems involving a wavy bottom.

Of particular interest are the frequencies for $\mu = 0$, at which the velocity potential is entirely given by the periodic factor and has spatial period λ_{bar} or $2\lambda_{bar}$. These frequencies are also the boundaries separating the wave modes with real and pure imaginary μ, corresponding to exponential and oscillatory modulation of the wave amplitude in space. Given $k_B h_0$, we can always write the flat-bottom ($\epsilon = 0$) frequencies ω_{Bm} for waves with wavenumber $k_{Bm} \equiv mk_B$, i.e. wavelength $\lambda = (2/m)\lambda_{bar}$, $m = 1, 2, 3, \ldots$. For the given $k_B h_0$, and for $\epsilon \neq 0$, two frequencies for $\mu = 0$ can be found, ω_m^{c-} and ω_m^{c+}, both approaching ω_{Bm} as $\epsilon \to 0$. In the plane (ω, ϵ), the regions bounded by $\omega_m^{c-}(\epsilon)$ and $\omega_m^{c+}(\epsilon)$ are referred to as the mth resonance tongues, after the vertex points $(\omega_{Bm}, 0)$. For ω inside a resonant tongue, μ is real for the wave modes and the wave amplitudes are modulated exponentially in x. Since such waves cannot exist in an open domain $-\infty < x < \infty$, these frequencies are said to be unstable (or 'forbidden' in physics). Such waves, however, have physical meaning on a finite domain of indefinite length, and are important for the phenomena of Bragg resonances in water waves (not the primary topic of this paper, but some remarks will be made in § 4). For ω outside a resonant tongue, μ is pure imaginary for the wave modes and the wave amplitudes are modulated sinusoidally. These are sometimes also viewed as 'quasi-periodic' in space.

Along the boundaries of the mth resonance tongue where $\mu = 0$, the motion has spatial period $2\lambda_{bar}$ or λ_{bar}, but as $\epsilon \to 0$ these waves approach the flat-bottom wave of wavelength $\lambda = (2/m)\lambda_{bar}$ (corresponding to ω_{Bm}), which for $m > 2$ is shorter than λ_{bar}. One might naturally ask if these waves actually have the shortest period $\lambda = (2/m)\lambda_{bar}$ along the boundaries of the mth tongue. This seems not to be case when $m > 2$. As will be seen in the examples that follow, for $m > 2$ there appear to be m cycles of a wave within a period of the periodic factor, all with 'local' wavelengths close to $\lambda = (2/m)\lambda_{bar}$ but none of them repeating the waveforms of others. It is only in the limit $\epsilon \to 0$ that they become identical.

We have considered a number of examples of bottom profiles with various ϵ and $k_B h_0$. Some profile functions are given in appendix C. The conformal maps are found using the method in appendix B and the resonant tongues for $m = 1, 2, 3$ and 4 are computed. Three cases are discussed here: (i) a simple sinusoidal profile $h_b(x) = \epsilon h_0 \cos 2k_B x$ with $k_B h_0 = 1.0$; (ii) a doubly sinusoidal profile $h_b(x) = \epsilon h_0 (\sin 4k_B x + \sin 6k_B x)$ with $k_B h_0 = 0.6545$; (iii) a square wave profile with rounded corners, $h_b(x)$ in (C 1) with $k_B h_0 = 0.5$. To fix the idea, we define the crest-to-trough height of bottom undulations as $2a_b = h_{b,max} - h_{b,min}$ and refer to a_b as the bottom amplitude. Thus, $a_b/h_0 = \epsilon, 1.9057\epsilon$ and 1.2810ϵ for cases (i)–(iii), respectively.

Sample plots of the bottom profiles are shown varying in $k_B x$ and in ξ, in figures 2(*a*), 3(*a*) and 4(*a*) with $a_b/h_0 = 0.5$, 0.7623 and 0.4484, respectively. The graph of $h_b(\xi)$ as a function of $x(\xi)$ is included, but is almost indistinguishable from that of $h_b(x)$ versus $k_B x$, indicating the accuracy of the map computed. In the mapping variable ξ, the bottom profile in general has flattened crests and sharpened troughs. As ϵ increases, the troughs become increasingly cusp-like, requiring more sampling points for applying the discrete Fourier transform in finding the map. The sampling

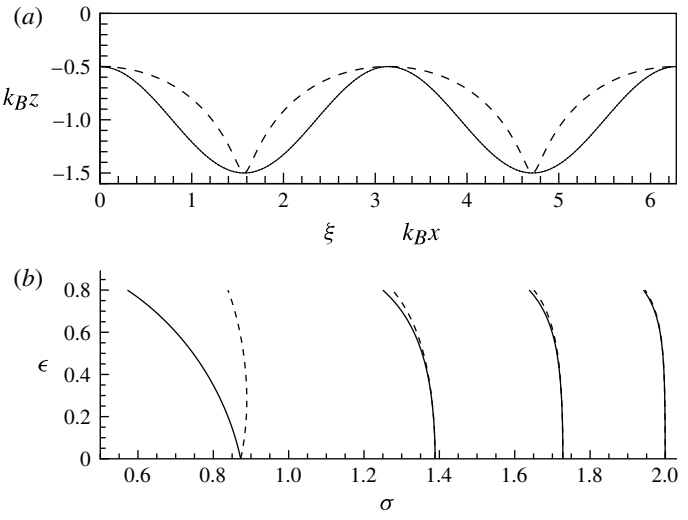

FIGURE 2. (*a*) Graphs of a simple sinusoidal bed $h_b(x) = \epsilon h_0 \cos 2k_Bx$, for $\epsilon = 0.5$ and $k_Bh_0 = 1.0$: ——, $h_b(x)$ versus k_Bx; – – –, $h_b(\xi)$ versus ξ; · · · · · ·, $h_b(\xi)$ versus $x(\xi)$ (indistinguishable from the solid curve). (*b*) Resonance tongues (unstable frequencies) for $m = 1, 2, 3$ and 4: ——, ω_m^{c-}; – – –, ω_m^{c+}. Frequency is normalized as in (2.13).

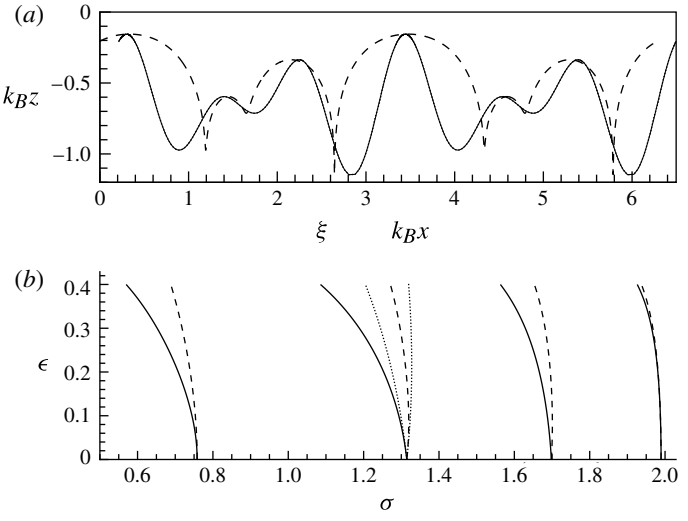

FIGURE 3. (*a*) Graphs of a doubly sinusoidal bed $h_b(x) = \epsilon h_0 [\sin(4k_Bx) + \sin(6k_Bx)]$, for $\epsilon = 0.4$ and $k_Bh_0 = 0.6545$: ——, $h_b(x)$ versus k_Bx; – – –, $h_b(\xi)$ versus ξ; · · · · · ·, $h_b(\xi)$ versus $x(\xi)$. (*b*) Resonance tongues (unstable frequencies) for $m = 1, 2, 3$ and 4: ——, ω_m^{c-}; – – –, ω_m^{c+}. Frequency is normalized as in (2.13). Dotted curves, $m = 1$ resonance tongue for $h_b = \epsilon h_0 \sin(4k_Bx)$.

points $N = 2^{10}$ are used for $\epsilon > 0.7$ ($a_b/h_0 > 0.7$) in case (i), $N = 2^{12}$ for $\epsilon > 0.35$ ($a_b/h_0 > 0.6670$) in case (ii) and $N = 2^{11}$ for $\epsilon > 0.3$ ($a_b/h_0 > 0.3843$) in case (iii). Note that $\Theta_j^{\pm}$ can be truncated maximally at $j = N/2$ because of the truncation of b_j and c_j: see (2.5). Therefore, the maximum dimensions of the matrix $\boldsymbol{A}$ obtained

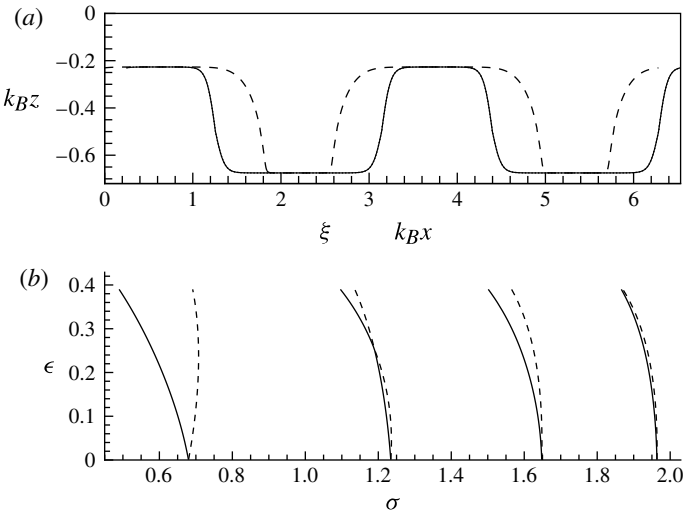

FIGURE 4. (a) Graphs of a square wave bed with rounded corners, for $h_b(x)$ given in (C 1), and $\epsilon = 0.35$ and $k_Bh_0 = 0.5$: ——, $h_b(x)$ versus k_Bx; – – –, $h_b(\xi)$ versus ξ; · · · · · ·, $h_b(\xi)$ versus $x(\xi)$. (b) Resonance tongues (unstable frequencies) for $m = 1, 2, 3$ and 4: ——, ω_m^{c-}; – – –, ω_m^{c+}. Frequency is normalized as in (2.13).

from (2.15) using the odd n representation are $N/2 \times N/2$, or $(N/2+1) \times (N/2+1)$ using the even n; correspondingly, the Fourier coefficients of the periodic factor can be determined for $D_{\pm n}$, $n = 1, 3, \ldots, N/2-1$, or $D_{\pm n}$, $n = 0, 2, \ldots, N/2$. However, because of the exponential convergence of $\Theta_j^{\pm}$ mentioned above, one can reduce the size of $\boldsymbol{A}$ without significantly affecting the result of (2.21). In various examples we have explored, we have tried to truncate $\Theta_j^{\pm}$ at $j = N/2$, $N/4$ and even $j = N/8$ for large N, and found essentially same results of (σ, μ) and D_n within the numerical accuracy.

Given a water depth k_Bh_0, the resonance tongues sweep towards low frequency as ϵ increases, due to the decrease of water depth k_Bh in the mapped plane: see figures 2(b), 3(b) and 4(b). The down-shift of frequency can be so significant that the flat-bottom resonance frequency ω_{Bm} (the vertex of a tongue) can be outside the resonance tongue even when ϵ is fairly small. This is consistent with the previous studies of a cusp-like bottom (HY07, YH10), in which k_Bh is fixed and the resonance tongues are seen to bend towards high frequencies as ϵ increases due to an increase of the corresponding k_Bh_0. For the sinusoidal bed, the resonance tongues for $m > 1$ are extremely narrow: see figure 2(b). Simple sinusoidal bed profiles are often used in asymptotic analyses considering small ϵ and slowly varying waves (e.g. Mei 1985; Yu & Mei 2000). Such analyses are illuminating in physics, but it will be difficult to extend them to higher orders for studying $m > 1$ resonances even when ϵ is small, due to the down-shift of frequency and the narrowness of the unstable regions.

The resonance tongues do not necessarily become narrower as m increases. For example, for the doubly sinusoidal bed, the resonance tongue for $m = 2$ is the largest, and those for $m = 1$ and $m = 3$ are comparable: see figure 3(b). For the square wave bed in figure 4(b), the resonance tongues for even m are smaller. Furthermore, the boundaries of the resonance tongue for $m = 2$ merge together as ϵ increases, reducing the tongue width to nearly zero, but become separated again as ϵ increases further.

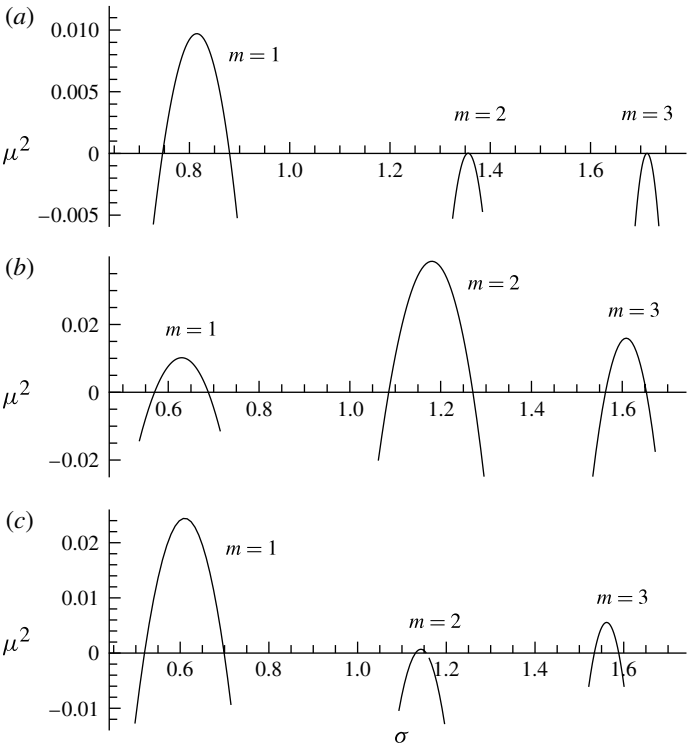

FIGURE 5. Graphs of μ^2 as a function of σ for wave modes near the $m = 1, 2$ and 3 resonance tongues: (*a*) for the simple sinusoidal bed in figure 2(*a*); (*b*) for the doubly sinusoidal bed in figure 3(*a*); (*c*) for the square wave bed in figure 4(*a*).

Similar behaviour is also seen for $m = 4$, except that the merging occurs at higher ϵ. Although the resonance tongues in this study have some features similar to those for the typical Mathieu equation, such as the sweeping cusp-like shape, this feature of merging and separating of the boundaries, to the best of our knowledge, has not been observed previously. However, for Hill's equations, it is known that in certain cases some, or even most, of the resonance tongues (or unstable intervals) may disappear: see Magnus & Winkler (1979) especially chapter 7.

Figure 5 shows μ^2 as a function of the dimensionless frequency σ for the wave modes. For σ outside a resonance tongue, $\mu^2 < 0$ as μ is pure imaginary; when inside, μ is real and $\mu^2 > 0$. To give a general idea, the periodic factors at the free surface $z = 0$ (i.e. $\eta = 0$) are plotted in figure 6 for the wave modes over the doubly sinusoidal bed in figure 3(*a*). The frequencies are $\sigma = 0.5430$, 0.5698, 0.6318, 0.6882 (with $\mu = 0.1049$i, 0, 0.1009, 0), corresponding to the outside, left boundary, middle and right boundary of the $m = 1$ resonance tongue, respectively. The surface elevation is $\mathrm{e}^{\mu\xi}P(\xi, 0; \mu)$, using the value of μ for each case. As is pointed out in HY07, the Floquet exponent μ for ξ is for $k_B x$ as well, and the periodic factors in the physical and mapped plane are related by $\mathrm{e}^{\mu k_B x}P_1(k_B x, k_B z; \mu) = \mathrm{e}^{\mu\xi}P(\xi, \eta; \mu)$, with P_1 and P having the same period. When $\mu = 0$, P_1 and P are the same. For completeness, the periodic factors at $z = 0$ for higher-frequency wave modes (with $\mu = 0$) are shown in figure 7. Along the boundaries for $m = 1$ and $m = 2$ tongues, the waves have exact wavelengths λ_{bar}/m: see figures 6(*b,d*) and 7(*a*). For $m = 3$ in figure 7(*b*), there are

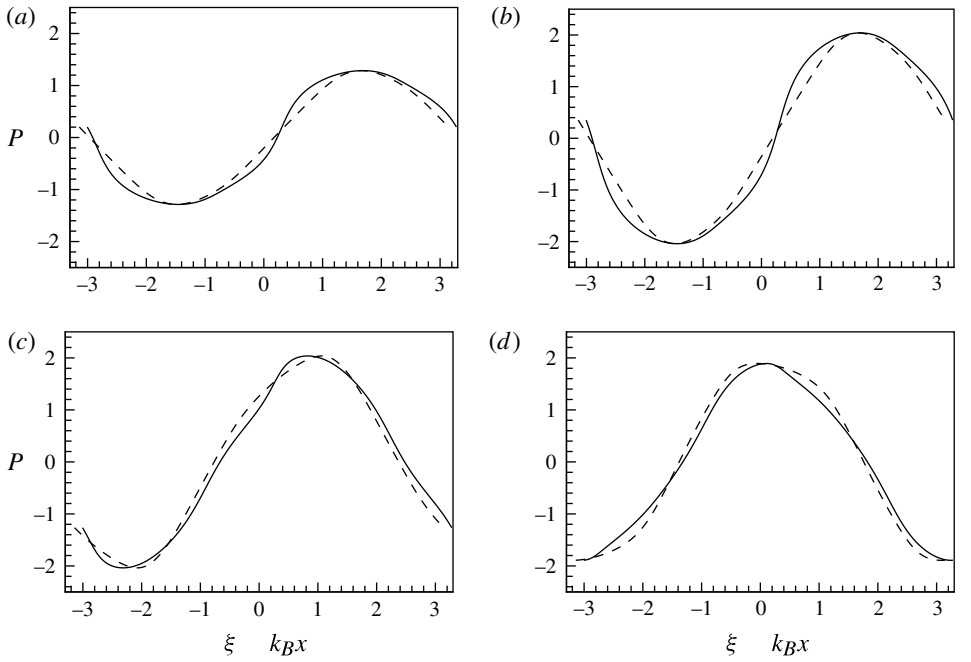

FIGURE 6. Periodic factor at $\eta = 0$ for the propagating wave mode over the doubly sinusoidal bed in figure 3(*a*): (*a*) $\sigma = 0.5430$, $\mu = 0.1049\mathrm{i}$; (*b*) $\sigma = 0.5698$, $\mu = 0$; (*c*) $\sigma = 0.6318$, $\mu = 0.1009$; (*d*) $\sigma = 0.6882$, $\mu = 0$. Lines: ——, P as a function of $k_B x$; – – –, P as a function of ξ.

three waves in an interval of 2π (period of the motion), all with wavelengths close to $2\pi/3$, but different. Similarly, for $m = 4$ in figure 7(*c*), the local wavelengths of individual waves are close to $2\pi/4$; as a result, the spatial pattern of the motion repeats after 2 waves, i.e. in period π of the periodic factor.

The Floquet exponents for the first three evanescent modes are listed in table 1 for $\sigma = 0.5698$ and $\sigma = 1.0856$. It is clear that the horizontal variation is essentially $\mathrm{e}^{\mu\xi}$ given the large real values of μ (and their negatives). For comparison, we include the eigenvalues of the flat-bottom evanescent modes for both depths $k_B h_0$ and $k_B h$, i.e. $\mu_{flat} = \kappa_n / k_B$, where $\omega^2 = -g\kappa_n \tan \kappa_n h$. The Floquet exponents are fairly close to the flat-bottom eigenvalues for the water depth $k_B h$ in the mapped domain, and significantly different from the values of μ_{flat} for the mean depth $k_B h_0$ in the physical domain (which are the limiting values as $\epsilon \to 0$).

4. Remarks on Bragg resonances by a periodic bottom

Although the resonance tongues are forbidden zones for waves travelling in $-\infty < x < \infty$, they are of great interest in studies of wave scattering in a finite domain. One of the examples is Bragg resonance of water waves by a finite patch of wavy bottom. In this case, a travelling wave with a frequency inside a resonance tongue becomes exponentially modulated over the patch due to the cumulative effects of reflections from successive bottom undulations. The phenomenon has been extensively studied in the literature because of its implications for coastal morphology and sediment processes: see Mei, Hara & Yu (2001) and references therein.

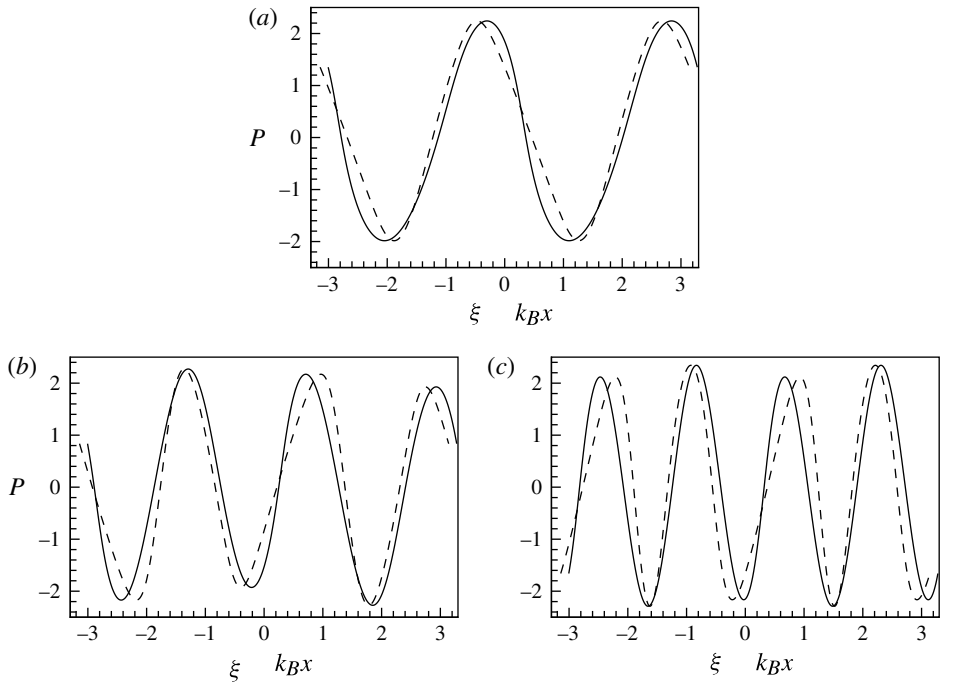

FIGURE 7. Periodic factor at $\eta = 0$ for higher-frequency wave mode over the doubly sinusoidal bed in figure 3(*a*): (*a*) $\sigma = 1.0856$, $\mu = 0$; (*b*) $\sigma = 1.5630$, $\mu = 0$; (*c*) $\sigma = 1.9262$, $\mu = 0$. Lines: ——, P as a function of k_Bx; – – –, P as a function of ξ.

$\sigma = 0.5698$			$\sigma = 1.0856$		
μ	μ_{flat1}	μ_{flat2}	μ	μ_{flat1}	μ_{flat2}
7.510622	7.510825	4.694487	7.221154	7.223535	4.400179
15.179226	15.179253	9.548043	15.041292	15.041564	9.409620
22.812136	22.812144	14.365440	22.720948	22.721027	14.274113

TABLE 1. The Floquet exponents μ of the first three evanescent modes for the doubly sinusoidal bed in figure 3(*a*), compared with the eigenvalues of the flat-bottom evanescent modes: μ_{flat1} is for $k_Bh = 0.4125$ and μ_{flat2} is for $k_Bh_0 = 0.6545$.

A very interesting and careful laboratory study of Bragg resonances was carried out by Guazzelli, Rey & Belzons (1992), who considered linear water waves propagating over the doubly sinusoidal beds. One of the bed forms was a sum of two equal-amplitude sine waves of wavelength 6 and 4 cm, i.e. wavenumbers $K_1 = \pi/3$ cm^{-1} and $K_2 = \pi/2$ cm^{-1} respectively. The fundamental (shortest) spatial period of the bed is therefore 12 cm (since 12 is the least common multiple of 6 and 4). Using our notation, $k_B = \pi/12$ cm^{-1}, making $K_1 = 4k_B$ and $K_2 = 6k_B$. This is the profile in case (ii) in § 3. Two sets of parameters were used in the experiments: $\epsilon = 0.25$ with $k_Bh_0 = 1.0472$ and $\epsilon = 0.4$ with $k_Bh_0 = 0.6545$.

Guazzelli *et al.* found three main peaks in the reflection coefficient upwave of a patch of these beds, near the frequencies corresponding to water waves (on a flat

bottom of the mean depth) of wavenumbers $\pi/12$, $\pi/6$ and $\pi/4$ cm^{-1}. They referred to the last two of these as the first-order ($m = 1$) Bragg reflections corresponding to $K_1/2$ and $K_2/2$, as if the two individual bed components, $\sin K_1 x$ and $\sin K_2 x$, were alone, and interpreted the first peak near $(K_2 - K_1)/2$ as a 'second-order subharmonic resonance'. Guazzelli *et al.* used the asymptotic theory of Mei (1985) to compute the reflection coefficients of the two sine bed components alone, and obtained individual resonance peaks which agreed fairly well with the last two peaks of the measurements. This seems to have suggested that the Fourier components of a bed can be viewed as acting independently. In the earlier literature (Kirby 1986; Mattioli 1990), superposing the results for individual bed components acting alone has been used. However, Kirby (1986) remarked that, away from the resonance peaks, the reflection coefficients from the result of superposition behave quite differently from that for the composite bed, indicating interactions among the bed components. It is emphasized in YH10 that one cannot interpret a $m > 1$ resonance of a general periodic bed as if it were the $m = 1$ resonance of its mth Fourier components $\cos(2mk_B x)$ and $\sin(2mk_B x)$, as there is no linearity with respect to the bottom shape even when the fluid motion is linear. To further stress this quantitatively, we include in figure 3 the $m = 1$ resonance tongue of $h_b(x) = \epsilon h_0 \sin(4k_B x)$, comparing with the $m = 2$ resonance tongue of the doubly sinusoidal bed. The difference is clear.

Guazzelli *et al.* also did numerical simulations of the flow over the actual bed form to calculate the reflection coefficients, and obtained good agreement over the whole range, in particular at the frequency corresponding to $(K_2 - K_1)/2$, the 'second-order subharmonic'. It seems pretty clear that if either the K_1 or K_2 Fourier component were removed from the actual bed form, one would not expect to see the peak at $(K_2 - K_1)/2$. In other words, one would not expect to produce a peak reflection close to $(K_2 - K_1)/2$ by linearly combining two numerical results, one for bottom $h_{b1} = \sin(K_1 x)$ and the other for $h_{b2} = \sin(K_2 x)$, which is a point emphasized in YH10. The fact that a peak at $(K_2 - K_1)/2$ is found both experimentally and numerically for a doubly sinusoidal bottom of which $(K_2 - K_1)$ is not even a component, indicates that the individual Fourier components indeed do not act independently, and that it is not appropriate to decompose the scattering problem with respect to the bed components.

Using the Floquet solutions in § 2, we identify the first-order ($m = 1$) Bragg resonance wavenumber $k_B = \pi/12$ cm^{-1}, given by the shortest period of the bottom, and the second and third resonance wavenumbers $k_{B2} = \pi/6$ cm^{-1} and $k_{B3} = \pi/4$ cm^{-1}. The flat-bottom frequencies associated with these wavenumbers, ω_{Bm}, are the vertices of the $m = 1$, 2 and 3 resonance tongues at $\epsilon = 0$. These can be readily verified in figure 3 for $k_B h_0 = 0.6545$, recalling that $\sigma = \omega/\sqrt{gk_B}$.

It is particularly interesting to note that a shift towards lower frequency than ω_{Bm} of the experimental resonance peaks was observed by Guazzelli *et al.* They also remarked that the shift increases for larger ϵ. This is consistent with the frequency down-shifting of resonance tongues as ϵ increases, which we observe from the Floquet solutions: see figures 2(*b*)–3(*b*). In figure 8 of Guazzelli *et al.* (1992) for $\epsilon = 0.4$ and $k_B h_0 = 0.6545$, all three main experimental resonance peaks are noticeably shifted to the low-frequency side of the corresponding flat-bottom Bragg frequencies (marked by the arrows labelled f_-, f_1 and f_2). By a close examination of that figure, we have estimated the frequencies of these experimental peaks. They are listed in table 2, together with the flat-bottom Bragg frequencies. For the Floquet solutions, it is seen in figure 3(*b*) that ω_{B1}, ω_{B2} and ω_{B3} are well outside the resonance tongues when $\epsilon = 0.4$, on the high-frequency side. It is expected that the peak of reflection coefficients is at or close to the centre of the appropriate resonance tongue where the maximum value

f_{obs} (Hz)	f_{exc} (Hz)	f_{flat} (Hz)
1.68	1.6044	1.9341
2.97	3.0156	3.3539
4.18	4.1045	4.3329

TABLE 2. The frequencies at the first three resonance peaks for the doubly sinusoidal bed, for $\epsilon = 0.4$ and $k_B h_0 = 0.6545$: f_{obs}, experimental data in figure 8 of Guazzelli *et al.* (1992); f_{exc}, the exact Floquet solutions; f_{flat}, the flat-bottom Bragg frequencies.

of μ occurs. These frequencies can be obtained from figure 5(*b*), and are included in table 2. The Floquet solutions compare very well with the experimental data at all three peaks. Furthermore, figure 5(*b*) predicts that the peak of reflection coefficients for the $m = 2$ resonance will be the greatest due to the large magnitude and broad range of real μ in that region, while the peak for $m = 3$ resonance will be the narrowest among the three. These features are similarly seen from the experimental data in figure 8 of Guazzelli *et al.*

For more quantitative and detailed comparisons, one must solve the boundary value problem of wave scattering by a patch of doubly sinusoidal bottom in an otherwise flat bed, following the method in Yu & Zheng (2012) but using the Floquet solutions in § 2.2. This is beyond the scope of this study and will not be pursued here.

5. Concluding remarks

We have developed an exact theory for linear time periodic motions over general periodic seabeds of arbitrary amplitude and shape. This utilizes a conformal map of the undisturbed flow domain to a strip with flat surface and bottom, thereby transferring the effects of a periodic seabed to the mapped free surface boundary condition. The exact solutions, to the linear problem in the mapped domain, are constructed as Floquet solutions. The determination of the Floquet exponents μ is described together with one possible algorithm to obtain the conformal map as a Fourier series. The latter is a fairly straightforward iteration using the fast Fourier transform.

We classify the Floquet solutions as 'propagating-wave-like' and 'evanescent-wave-like' solutions, based on their behaviours at the limit when the bottom amplitude $\epsilon \to 0$ (the flat bottom limit). We have indeed found a set of Floquet solutions which approaches the complete set of linear solutions of a flat bottom for the given frequency as $\epsilon \to 0$. Thus, these Floquet solutions are the analogues, for a general periodic bottom, of the propagating and evanescent waves over a flat bottom, and form the basis for solutions to various boundary value problems involving a wavy bottom. The resonance tongues, i.e. unstable frequencies for wave modes, are found to have some general features similar to those for a typical Mathieu equation, e.g. sweeping cusp-like shape. Given a mean water depth, the resonance tongues sweep towards low frequency as ϵ increases. This is clearly explained by the decrease of water depth in the mapped domain as ϵ increases. The detailed structures of resonance tongues, however, can be quite varied and complex, depending on the bottom topographies. For instance, for a square wave bed, a resonance tongue may reduce to nearly zero width as ϵ increases to a finite value and open up again to a finite width with further increase of ϵ. Implications of such behaviours, in particular when the nonlinearity of the free surface is included, are worth investigating. Fairly good agreement has

been observed between the exact solutions and experimental data, in particular the down-shift of resonance frequencies with increasing bottom amplitude. More detailed comparisons can be carried out once the appropriate boundary value problem is solved using the exact solutions provided here.

Acknowledgements

We thank two anonymous reviewers whose comments helped to improve the paper. Support of J.Y. by the US National Science Foundation (Grants CBET-0756271 and CBET-0845957), during the period of this work, is gratefully acknowledged.

Appendix A. The reality of $\Delta(\mu, \sigma)$ for real μ

For $n =$ odd and the elements of vector $\boldsymbol{X}$ arranged as in (2.19), the matrix $\boldsymbol{A}$ is in (2.20). Taking the complex conjugate of each element A_{ij} and recalling that $\Theta_j^{+*} = \Theta_j^-$, we obtain a new matrix:

$$\widetilde{\boldsymbol{A}} = \begin{pmatrix} \cdots & \cdots & \cdots & \cdots & \cdots & \cdots \\ \cdots & L_{-3}^* & -\Theta_1^- & -\Theta_2^- & -\Theta_3^- & \cdots \\ \cdots & -\Theta_1^+ & L_{-1}^* & -\Theta_1^- & -\Theta_2^- & \cdots \\ \cdots & -\Theta_2^+ & -\Theta_1^+ & L_1^* & -\Theta_1^- & \cdots \\ \cdots & -\Theta_3^+ & -\Theta_2^+ & -\Theta_1^+ & L_3^* & \cdots \\ \cdots & \cdots & \cdots & \cdots & \cdots & \cdots \end{pmatrix}. \tag{A 1}$$

For real μ, $L_{-n}^*(\mu) = L_n(\mu)$. Thus, (A 1) becomes

$$\widetilde{\boldsymbol{A}} = \begin{pmatrix} \cdots & \cdots & \cdots & \cdots & \cdots & \cdots \\ \cdots & L_3 & -\Theta_1^- & -\Theta_2^- & -\Theta_3^- & \cdots \\ \cdots & -\Theta_1^+ & L_1 & -\Theta_1^- & -\Theta_2^- & \cdots \\ \cdots & -\Theta_2^+ & -\Theta_1^+ & L_{-1} & -\Theta_1^- & \cdots \\ \cdots & -\Theta_3^+ & -\Theta_2^+ & -\Theta_1^+ & L_{-3} & \cdots \\ \cdots & \cdots & \cdots & \cdots & \cdots & \cdots \end{pmatrix}. \tag{A 2}$$

It is readily seen that the system $\widetilde{\boldsymbol{A}}\widetilde{\boldsymbol{X}} = 0$, where

$$\widetilde{\boldsymbol{X}} = [\cdots \; D_3 \;\; D_1 \;\; D_{-1} \;\; D_{-3} \;\; \cdots]^{\mathrm{T}}, \tag{A 3}$$

represents a set of linear equations identical to $\boldsymbol{AX} = 0$, except for rearranging the equations and vector elements D_n. Therefore, $\widetilde{\boldsymbol{A}}$ and $\boldsymbol{A}$ must have the same set of eigenvalues. Since the determinant of a matrix equals the product of the eigenvalues of the matrix, we must have $\det(\boldsymbol{A}) = \det(\widetilde{\boldsymbol{A}})$. However, $\det(\widetilde{\boldsymbol{A}}) = \det(\boldsymbol{A})^*$, as $\widetilde{A}_{ij} = A_{ij}^*$. Thus, $\det(\boldsymbol{A}) = \det(\boldsymbol{A})^*$, implying that $\det(\boldsymbol{A})$ must be real. This proves that $\Delta(\mu, \sigma)$ is real when μ is real.

Appendix B. A numerical scheme for computing the conformal map

Let $z_b \equiv -h_0 + h_b(x)$. Given a seabed z_b, we find b_n and c_n by iterations and applying the fast Fourier transform (FFT) on $z_b(x)$ in ξ at each step. From (2.5) and (2.6), we

write

$$k_B x = \xi + \epsilon k_B h \sum_{n=1}^{\infty} \left[\frac{1}{2} \mathrm{i} \, (b_n - \mathrm{i} c_n) \, \mathrm{e}^{\mathrm{i}2n\xi} - \frac{1}{2} \mathrm{i} \, (b_n + \mathrm{i} c_n) \, \mathrm{e}^{-\mathrm{i}2n\xi} \right] \coth 2nk_B h, \quad \text{(B 1)}$$

$$k_B z_b = -k_B h + \epsilon k_B h \sum_{n=1}^{\infty} \frac{1}{2} \, (b_n - \mathrm{i} c_n) \, \mathrm{e}^{\mathrm{i}2n\xi} + \frac{1}{2} \, (b_n + \mathrm{i} c_n) \, \mathrm{e}^{-\mathrm{i}2n\xi}, \quad \text{(B 2)}$$

using the complex notations for convenience to work with the discrete Fourier transform.

Let $\xi_j = \Delta(j-1), j = 1, 2, \ldots, N$ be the sampling points, where the sampling interval $\Delta = \pi/N$. Note that $N = 2^p$ for use of the standard FFT. The sampled values are $z_{bj} = -h_0 + h_b(x(\xi_j))$, where $x(\xi_j)$ is evaluated from (B 1) at ξ_j. The discrete Fourier transform of the N points z_{bj} is

$$Z_n = \sum_{j=1}^{N} z_{bj} \mathrm{e}^{-\mathrm{i}2\pi(j-1)(n-1)/N} = \sum_{j=1}^{N} z_{bj} \mathrm{e}^{-\mathrm{i}2\xi_j(n-1)}, \quad \text{(B 3)}$$

and the inverse Fourier transform that recovers the set of z_{bj} exactly from Z_n is

$$z_{bj} = \frac{1}{N} \sum_{n=1}^{N} Z_n \mathrm{e}^{\mathrm{i}2\pi(j-1)(n-1)/N} = \frac{1}{N} \sum_{n=1}^{N} Z_n \mathrm{e}^{\mathrm{i}2\xi_j(n-1)}. \quad \text{(B 4)}$$

Note that $Z_n = Z^*_{n+N/2}$, $n = 2, 3, \ldots, N/2$, since z_b is real; Z_1 corresponds to the zeroth wavenumber and $Z_{1+N/2}$ is for the Nyquist critical frequency (wavenumber) of the sampling. Truncating the series in (B 2) and comparing it with (B 4), we get

$$\left.\begin{aligned} &-k_B h = \frac{1}{N} Z_1, \quad \frac{1}{2} \, (b_n - \mathrm{i} c_n) \, \epsilon k_B h = \frac{1}{N} Z_{n+1}, \quad n = 1, 2, \ldots N/2 - 1, \\ &(\epsilon k_B h) b_{N/2} = \frac{1}{N} Z_{N/2+1}, \quad c_{N/2} = 0. \end{aligned}\right\} \quad \text{(B 5)}$$

The iteration is as follows. At the kth step, we evaluate $x^{k-1}(\xi_j)$ from (B 1) using b_n^{k-1} and c_n^{k-1}, and get $z_{bj}^{k-1} = -h_0 + h_b(x^{k-1}(\xi_j))$. Applying the FFT on z_{bj}^{k-1} and using (B 5), we obtain the updates b_n^k and c_n^k. From the inverse FFT (B 4), we get a set of estimated values z_{bj}^k. The iteration continues until the mean square error between z_{bj}^k and z_{bj}^{k-1} reduces to a prescribed tolerance. We begin the iteration with $b_n = c_n = 0$ (i.e. $k_B x = \xi$ initially).

The method described above is an explicit scheme. It converges fairly fast when $h_b(x)$ is smooth or ϵ is small. For large ϵ and not-so-smooth functions, modifications may be needed to improve the convergence, for instance using $\widetilde{b}_n^k = (b_n^k + b_n^{k-1})/2$ and $\widetilde{c}_n^k = (c_n^k + c_n^{k-1})/2$ as the updates for the kth step, or some other forms of weighted average if necessary. We have tried a number of profiles (some are not included in this paper) and found the maps for large ϵ in various water depths. For unsmooth functions (e.g. the square wave profile) and with large ϵ, the convergence can be slow due to the large N needed. The numerical method can be improved to increase the efficiency for computing the map, but it is beyond the scope of this study.

Appendix C. Bottom profiles

Since $h_b(x + \pi) = h_b(x)$, we only give the bottom profile $h_b(x)$ in one period for $0 \leqslant x \leqslant \pi$, as follows.

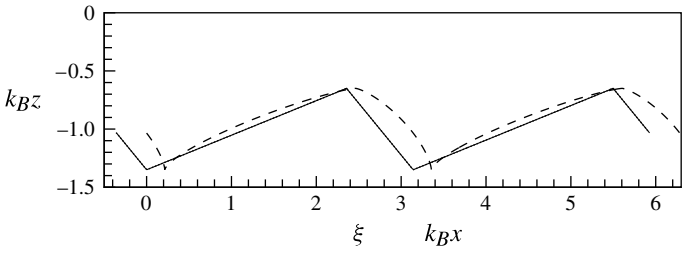

FIGURE 8. Graphs of a sawtooth bed profile, for $\epsilon = 0.7$ and $k_Bh_0 = 1.0$: ——, $h_b(x)$ versus k_Bx; – – –, $h_b(\xi)$ versus ξ; · · · · · ·, $h_b(\xi)$ versus $x(\xi)$.

C.1. *Square wave with rounded corners*

$$h_b(x) = \begin{cases} c\tanh(b_2x) & \text{for } 0 \leqslant x < a/2, \\ c\tanh[b_2(a-x)] & \text{for } a/2 \leqslant x < a, \\ \tanh[b_1(a-x)] & \text{for } a \leqslant x < (\pi+a)/2, \\ \tanh[b_1(x-\pi)] & \text{for } (\pi+a)/2 \leqslant x < \pi. \end{cases} \tag{C 1}$$

The width of the upper square above the mean level is given by a, and thus the width of the lower square is $\pi - a$. The smoothness of the top and bottom corners can be adjusted, respectively, using b_1 and b_2. For $h_b(x)$ to have zero average in x,

$$c = \frac{b_2}{b_1}\frac{\ln[\cosh(b_1(a-\pi)/2)]}{\ln[\cosh(b_2a/2)]}. \tag{C 2}$$

The crest-to-trough height of the corrugations is $1 + c$. For the example used in § 3, $a = 0.4$, $b_1 = b_2 = 10$ and $c = \ln[\cosh 3\pi] / \ln[\cosh 2\pi]$, i.e. $1 + c = 2.5620$.

C.2. *Triangle and sawtooth waves*

$$h_b(x) = \begin{cases} x/a - c & \text{for } 0 \leqslant x < a, \\ -(x-2b)/(2b-a) - c & \text{for } a \leqslant x < 2b, \\ -c & \text{for } 2b \leqslant x < \pi. \end{cases} \tag{C 3}$$

The width of the triangle elements is $2b$; the spacing between two adjacent triangles (the flat section) is thus $\pi - 2b$. The skewness, or asymmetry, of the triangle is adjusted by a. When $a = b$ we have symmetrical triangle elements. For $h_b(x)$ to have zero average in x, $c = b/\pi$. The crest-to-trough height of the corrugations (i.e. the height of triangles) is 1. Note that $b \leqslant \pi/2$. When $b = \pi/2$ we have the sawtooth-shaped bottom corrugations (i.e. zero spacing between triangles), see figure 8 with $a = 3\pi/4$. The dotted curve $h_b(\xi)$ versus $x(\xi)$ is indistinguishable from the curve $h_b(x)$ versus k_Bx, indicating the accuracy of the map computed (with $N = 2^{11}$).

C.3. *Half-sine wave*

Replacing the symmetric triangle by a half-cycle of a sine function, we have the half-sine wave profile:

$$h_b(x) = \begin{cases} \sin(bx) - 2(\pi b)^{-1} & \text{for } 0 \leqslant x < \pi/b, \\ -2(\pi b)^{-1} & \text{for } \pi/b \leqslant x < \pi. \end{cases} \tag{C 4}$$

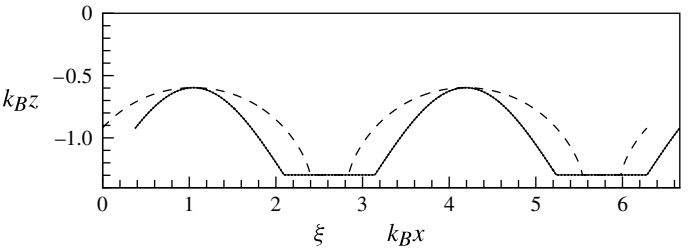

FIGURE 9. Graphs of a half-sine bed profile, for $\epsilon = 0.7$ and $k_Bh_0 = 1.0$: ——, $h_b(x)$ versus k_Bx; – – –, $h_b(\xi)$ versus ξ; · · · · · ·, $h_b(\xi)$ versus $x(\xi)$.

The width of the half-sine is π/b, where $b \geqslant 1$. The crest-to-trough height of the corrugations is 1. An example is given in figure 9 with $b = 1.5$. $N = 2^{11}$ is used. A special case is $b = 1$ where the flat section between two adjacent half-sines has zero width and the corrugations become upside-down cusps.

REFERENCES

AHLFORS, L. 1953 *Complex Analysis*. McGraw-Hill.

ATHANASSOULIS, G. A. & BELIBASSAKIS, K. A. 1999 A consistent coupled-mode theory for the propagation of small-amplitude water waves over variable bathymetry regions. *J. Fluid Mech.* **389**, 275–301.

DAVIES, A. G. 1982 The reflection of wave energy by undulations on the seabed. *Dyn. Atmos. Oceans* **6**, 207–232.

DEVILLARD, P., DUNLOP, F. & SOUILLARD, B. 1988 Localization of gravity waves on a channel with a random bottom. *J. Fluid Mech.* **186**, 521–538.

EVANS, D. V. & LINTON, C. M. 1994 On step approximations for water-wave problems. *J. Fluid Mech.* **278**, 229–249.

GUAZZELLI, E., REY, V. & BELZONS, M. 1992 Higher-order Bragg reflection of gravity surface waves by periodic beds. *J. Fluid Mech.* **245**, 301–317.

HEATHERSHAW, A. D. 1982 Seabed–wave resonance and sand bar growth. *Nature* **296**, 343–345.

HOWARD, L. N. & YU, J. 2007 Normal modes of a rectangular tank with corrugated bottom. *J. Fluid Mech.* **593**, 209–234.

JEFFREYS, H. & JEFFREYS, B. S. 1950 *Methods of Mathematical Physics*, 2nd edn. Cambridge University Press.

KIRBY, J. T. 1986 A general wave equation for waves over rippled beds. *J. Fluid Mech.* **162**, 171–186.

MAGNUS, W. & WINKLER, S. 1979 *Hill's Equation*. Dover.

MATTIOLI, F. 1990 Resonance reflection of a series of submerged breakwaters. *Il Nuovo Cimento* **13C**, 823–833.

MEI, C. C. 1985 Resonant reflection of surface water waves by periodic sandbars. *J. Fluid Mech.* **152**, 315–337.

MEI, C. C., HARA, T. & YU, J. 2001 Longshore bars and Bragg resonance. In *Geomorphological Fluid Mechanics* (ed. N. Balmforth & A. Provenzale), *Lecture Notes in Physics*, vol. 582, chap. 20, pp. 500–527. Springer.

NACHBIN, A. 1995 The localization length of randomly scattered water waves. *J. Fluid Mech.* **296**, 353–372.

NACHBIN, A. & PAPANICOLAOU, G. C. 1992 Water waves in shallow channels of rapidly varying depth. *J. Fluid Mech.* **241**, 311–332.

O'HARE, T. J. & DAVIES, A. G. 1992 A new model for surface wave propagation over undulating topography. *Coast. Engng* **18**, 251–266.

PORTER, R. & PORTER, D. 2003 Scattered and free waves over periodic beds. *J. Fluid Mech.* **483**, 129–163.

REY, V. 1992 Propagation and local behavior of normal incident gravity waves over varying topographies. *Eur. J. Mech.* B **11**, 213–232.

WHITTAKER, E. T. & WATSON, G. N. 1927 *A Course of Modern Analysis*, 4th edn. Cambridge University Press.

YU, J. & HOWARD, L. N. 2010 On higher order Bragg resonance of water waves by bottom corrugations. *J. Fluid Mech.* **659**, 484–504.

YU, J. & MEI, C. C. 2000 Do longshore bars shelter the shore? *J. Fluid Mech.* **404**, 251–268.

YU, J. & ZHENG, G. 2012 Exact solutions for wave propagation over a patch of large bottom corrugations. *J. Fluid Mech.* (in press).

ZHENG, G. 2011 Exact solutions for linear water wave scattering by a patch of finite amplitude periodic corrugations on a seabed. MSc thesis, Department of Civil, Construction and Environmental Engineering, North Carolina State University.